


ITC 4/51 Information Technology and Control Vol. 51/ No. 4 / 2022 pp. 704-722 DOI 10.5755/j01.itc.51.4.30858	Ensembling Scale Invariant and Multiresolution Gabor Scores for Palm Vein Identification	
	Received 2022/03/05	Accepted after revision 2022/08/10
	 http://dx.doi.org/10.5755/j01.itc.51.4.30858	

HOW TO CITE: Ananthi, G., Sekar, J. R., Arivazhagan, S. (2022). Ensembling Scale Invariant and Multiresolution Gabor Scores for Palm Vein Identification. *Information Technology and Control*, 51(4), 704-722. <http://dx.doi.org/10.5755/j01.itc.51.4.30858>

Ensembling Scale Invariant and Multiresolution Gabor Scores for Palm Vein Identification

G. Ananthi, J. Raja Sekar, S. Arivazhagan

Department of CSE, Mepco Schlenk Engineering College, Sivakasi, India;

e-mails: ananthi@mepcoeng.ac.in; jrsekar@mepcoeng.ac.in; sarivu@mepcoeng.ac.in

Corresponding author: ananthi@mepcoeng.ac.in

Biometric recognition based on palm vein trait has the advantages of liveness detection and high level of security. An improved human palm vein identification system based on ensembling the scores computed from scale invariant features and multiresolution adaptive Gabor features is proposed. In the training phase, from the input palm vein images, the interested palm regions are segmented using 3-valley point maximal palm extraction strategy, an improved method that extracts the maximal region of interest (ROI) easily and properly. Extracted ROI is enhanced using contrast limited adaptive histogram equalization method. From the enhanced image, local invariant features are extracted by applying scale invariant feature transform (SIFT). The texture and multiresolution features are extracted by employing adaptive Gabor filter over the enhanced image. These two features, scale invariant and multiresolution Gabor features act as the templates. In the testing phase, for the test images, ROI extraction, image enhancement, and two different feature extractions are performed. Using cosine similarity and match count-based classification, the score, S_s is computed for the SIFT features. Another score, S_g is computed using the normalized Hamming distance measure for the Gabor features. Both these scores are ensembled using the weighted sum rule to produce the final score, S_F for identifying the person. Experiments conducted with CASIA multispectral palmprint image database version 1.0 and VERA palm vein database show that, the proposed method achieves equal error rate of 0.026% and 0.0205% respectively. For these databases, recognition rate of 99.73% and 99.89% respectively are obtained which is superior to the state-of-the-art methods in authentication and identification. The proposed work is suitable for applications wherein the authenticated person should not be considered as imposter.

KEYWORDS: 3-valley point strategy, contrast limited adaptive histogram equalization, SIFT features, adaptive Gabor filter, normalized Hamming distance.

1. Introduction

Highly secure human recognition is more essential for today's electronic world. Jain et al. [22] stated that biometrics is a way to recognize or automatically identify the human beings based on either their physiological or behavioural characteristics. Earlier authentication methods are password mechanism, which needs the remembrance and card-based authentication, requires carrying the card for authentication. These traditional methods are not suitable for now-a-days because they can be easily broken (passwords) or stolen (cards) by the attackers. Out of the existing biometrics such as fingerprint, face, iris, retina, hand geometry, veins (finger, hand, and palm), gait, handwriting, and voice, palm vein is an interesting biometric because of its high security nature, liveness detection, uniqueness, user comfort and acceptability. Palm vein recognition is a biometric authentication method which uses the image processing and pattern recognition techniques to verify the persons based on their palm vein trait. Palm vein images are captured with near-infrared (NIR) wavelength light source. The complex pattern in the captured palm image shows the blood flow pattern of the user. Cross and Smith [13] and Wang et al. [63] concluded that the dark pixels in the image are because of the absorption of the infrared light by the blood. The entire image will vanish when the person is dead since there is no blood flow as mentioned by Arakala et al. [5]. As the palm vein is under the palm skin, it cannot be easily stolen or damaged by any intruders there by more secured biometric. Lee [33] and Zhou and Kumar [85] concluded that palm vein image acquisition is easy and comfortable to the users as it is non-intrusive. Since there is no direct contact with the palm vein image acquisition sensor, there are no hygiene issues, and the fear of contamination to the users' hands. So, the user acceptability is high to this biometric. Hawkes et al. [20], Kong and Zhang [29], MacGregor and Welford [40], Masaki Watanabe et al. [41], Wang et al. [62] and Wilson [66] highlighted that the palm vein pattern is unique for different individuals even for the twins. Yoruk et al. [73] insisted that palm vein is long lasting over the period of life. Palm vein authentication and identification can be used in variety of applications like finance transactions, access control, attendance, and customer verification.

The organization of this paper is as follows: Section 2 discusses the literatures related to the proposed work

whereas section 3 elaborates all the modules of the proposed work. Experimental results are discussed in section 4. Section 5 provides the conclusion.

2. Related Work

Based on the type of features extracted, the existing methods for personal authentication from the input palm vein images are broadly categorized into geometry-based, texture-based, local invariant-based, wavelet-based, deep learning-based and multibiometric approaches.

Geometry-based approaches introduced by Cho et al. [12], Greitans et al. [16], Hernández-García et al. [21], Kilian et al. [28], Lee [32, 33], Moravec [45], Wang et al. [64], Wu et al. [67, 69, 70], Zhang et al. [75], Zhou and Kumar [84, 85] are based on the geometrical locations of the vein pattern. Feature extraction methods such as local thresholding, multiscale matched filtering, complex matched filtering, localized Radon transform, directional coding, directional filter bank, etc., are geometry-based approaches.

Palm vein images are rich in texture which is formed based on the blood vessel patterns. Methods such as Gabor filter, local binary pattern, local derivative pattern, and binarized statistical image features descriptor method are used in texture-based approaches. The authors Al-Zubi et al. [3], Babalola et al. [7], Deepamalar and Madheswaran [14], Han and Lee [19], Kang and Wu [27], Ma et al. [39], Mirmohamadsadeghi and Drygajlo [44], Piciuccio et al. [51], and Wang et al. [65] used these texture-based approaches for palm vein authentication.

Invariant feature extraction methods that were used by Al-Zubi et al. [3], Balasubramanian and Raja Sekar [8], Chengathir Selvi and Muneeswaran [11], Kang et al. [26], Moravec [45], Muneeswaran et al. [46], Pan and Kang [48], Wang and Han [61] and Yan et al. [72] are highly appreciated while working with contact-free image acquisition systems. Scale invariant feature transform (SIFT), speeded-up robust features (SURF) and affine-SIFT (ASIFT), and RootSIFT are some of the local invariant feature extraction methods.

Wavelet-based methods which were introduced by Al-juboori et al. [2], Ananthi et al. [4], Arivazhagan et

al. [6], Elnasir et al. [15], Li et al. [35], Raja Sekar et al. [54], Toh et al. [59], Wu et al. [68] extract multiresolution features by applying wavelets such as Haar wavelet, wavelet locality preserving projection, and Morlet wavelet. All the salient features of the palm vein images at different resolutions are extracted by these methods. In our earlier work, Ananthi et al. [4] curvelet multiresolution transform was used.

Convolutional neural network (CNN), deep CNN (DCNN), AlexNet, and visual geometry group (VGG) are the deep learning models used for palm vein recognition by Jia et al. [23], Obayya et al. [47], Pan et al. [49], Qin et al. [52], Stanuch et al. [55], Zhong et al. [82]. These methods lead to good results while dealing with a huge volume of data. Zheng et al. [76-80] worked on data augmentation methods with deep learning techniques.

Multibiometric methods combine information received from multiple traits, multiple sensors, and multiple algorithms to improve the recognition accuracy. The authors Chen et al. [10], Li et al. [36], Michael et al. [42], Wang and Han [61], Wang et al. [62], Zhang et al. [74], and Zhou et al. [83] used multibiometric methods. Palmprint and palm vein traits were collectively used for person authentication. Other combinations of traits such as iris, palm vein, and finger vein were also introduced.

Generally all the existing palm vein recognition systems include the modules such as segmenting region of interest, feature extraction, feature matching and decision making. Gupta and Gupta [17, 18], Han and Lee [19], Joardar et al. [24] and Lee [33] adopted median filter for removing the salt-and-pepper noise and speckles. Mirmohamadsadeghi and Drygajlo [43] and Zhou and Kumar [85] used histogram equalization method to normalize and enhance palm vein images. Han and Lee [19], Lee [32] and Wu et al. [67] computed the background illumination as the local mean intensity and subtracted it from the original palm vein image to obtain the enhanced image. Kang and Wu [27] normalized the palm vein images using bilinear gray value differential method. Ananthi et al. [4] and Yan et al. [72] applied Difference of Gaussian and histogram equalization strategy (DoG-HE) for palm vein image enhancement. Gupta and Gupta [17], Joardar et al. [24, 25], Ma et al. [39], Qiu et al. [53], Thillainayagi and Senthil Kumar [58] and Yakno et al. [71] employed contrast limited adaptive histogram equalization method (CLAHE) [86] for improving the contrast of the image.

Lin and Fan [37] extracted multiple features such as mean, moment, and counter filters from palm dorsal vein images using multiresolution analysis with multiresolution filters. Unique feature called "Laplacian-palm" was extracted by Wang et al. [62] on the palmprint and palm vein fused images by applying locality preserving projection. Su [56] extracted the geometrical features from the ROI by aligning all the palm images to the same position by performing image rotation, shifting and interpolation. Vein bifurcation and ending features were obtained by applying Mexican hat operator in the ROI and minutiae features by Delaunay triangulation by Kumar and Venkata Prathyusha [30]. Zhou and Kumar [85] extracted palm vein features by using Hessian phase approach whereas Han and Lee [19], Lee [32] and Ma et al. [39] used Gabor filter approach. Wu et al. [67] used directional filter bank approach for line feature extraction from vein image. Kang et al. [27] used maximal principal curvature algorithm and k-means methodology for texture extraction. Balasubramanian and Raja Sekar [8], Joardar et al. [25], Phalguni [50] and Yan et al. [72] used SIFT algorithm for local invariant feature extraction. Chengathir Selvi and Muneeswaran [11] and Muneeswaran et al. [46] used local invariant features for recognition. Arivazhagan et al. [6] and Raja Sekar et al. [54] extracted multiresolution features. Wu et al. [68] extracted the subspace feature of the palm vein by using Haar-wavelet decomposition and partial least squares algorithm.

Kumar et al. [30] calculated two different matching scores namely cumulative and shape matching score. Final matching score was the weighted combination of these matching scores. Han and Lee [19], Kang and Wu [27], Lee [32], Ma et al. [39], Sun and Abdulla [57], Wu et al. [67, 68], Zhixian and Qiang [81] and Zhou and Kumar [85] followed distance-based feature matching. Li et al. [34] used nearest-neighbour classifier; Yan et al. [72] applied Hellinger Kernel over the RootSIFT features.

Normally contactless biometric traits suffer from image translation, rotation, and scaling variations. As SIFT features are invariant to these variations, the authors are motivated to use this transform and Gabor filter, a multiresolution filter, with an improved ROI extraction method.

The highlights of the proposed work are as follows:

- a Extracting the largest possible region of interest from the input palm vein image by using an im-

proved 3-valley point maximal palm extraction strategy.

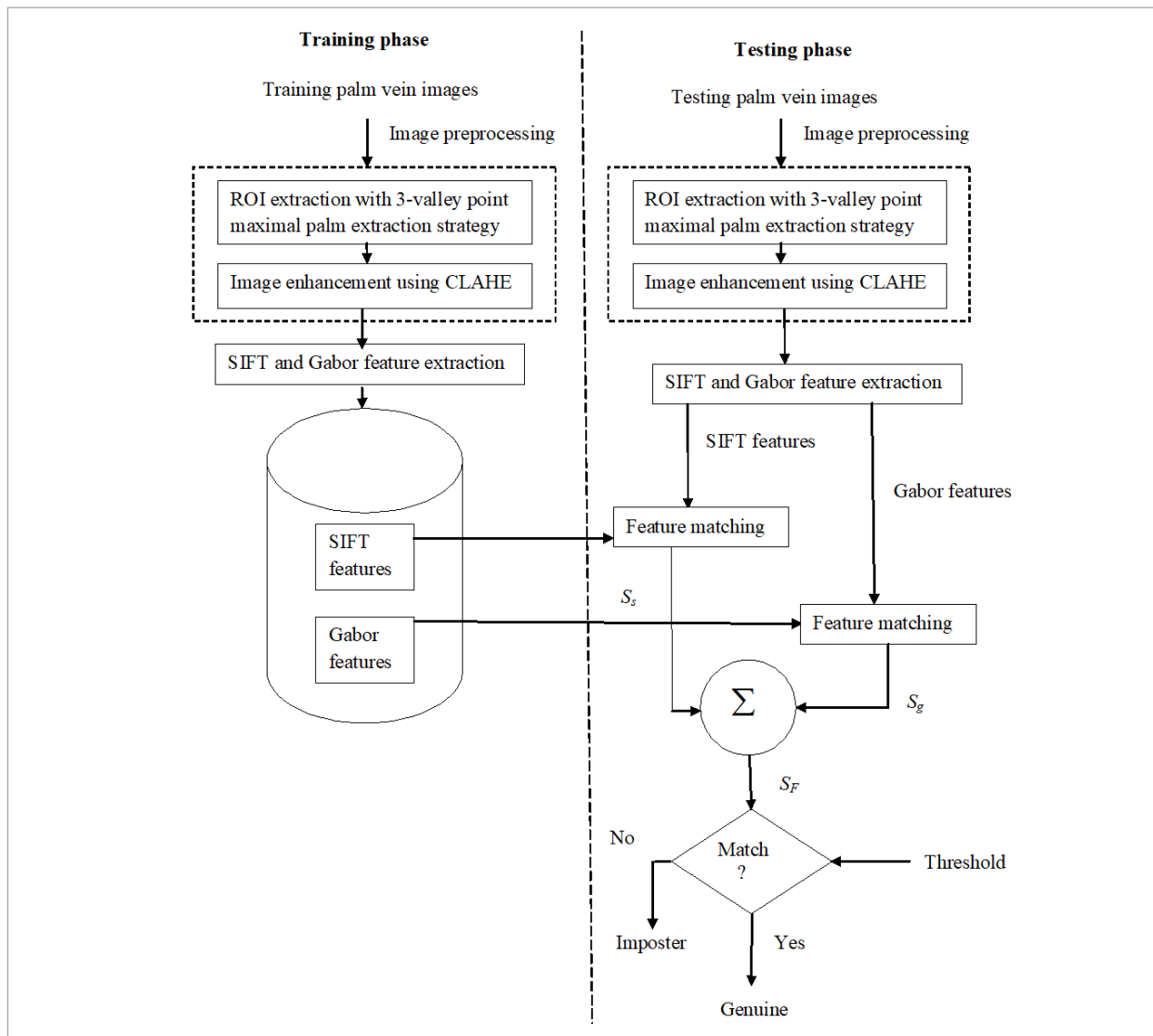
- b Scale invariant SIFT features and Gabor multiresolution features are extracted from the CLAHE enhanced palm image.
- c Matching over the SIFT and Gabor features result in two different score namely, S_s and S_g .
- d The palm vein identification system performance is appreciably improved by ensembling these scores using weighted sum rule to yield the final score, S_F .

3. Proposed Work

The proposed palm vein recognition system consists of five modules namely region of interest extraction, enhancing the ROI, extracting the features, feature matching and decision making. The steps, region of interest extraction and enhancing the ROI are collectively known as image preprocessing step. The schematic diagram of the proposed palm vein identification system is shown in Figure 1.

Figure 1

Schematic diagram of the proposed system

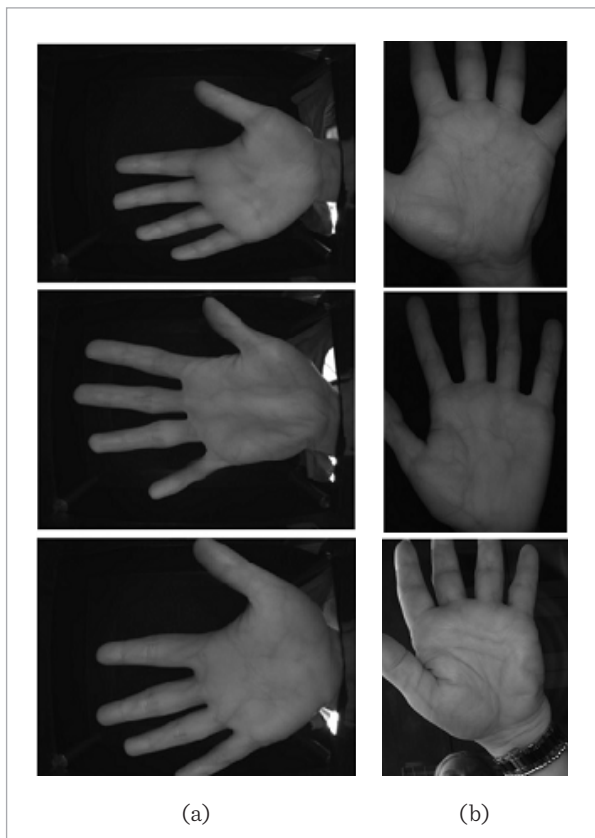


The proposed human identification system involves two phases – training and testing phase. During training phase, the users are registered to the authentication / identification system by storing the templates of features. During testing phase, the user is authenticated / identified by comparing the currently extracted features against the registered templates. i.e., for the test images, ROI extraction, image enhancement, and two different feature extractions are performed. A score, S_s is computed using cosine similarity and match count-based classification over the SIFT features and another score, S_g is computed using NHD over the Gabor features. These two scores are ensemble, and the final score, S_F is computed using weighted sum rule.

The score, S_F is used in decision making and identifying the human. Sample palm vein images from CASIA and VERA palm vein databases are shown in Figure 2(a) and 2(b) respectively.

Figure 2

Sample palm vein images (a) From CASIA MS palmprint image database V1.0 (b) From Vera palm vein database



3.1. Region of Interest Extraction

Region of interest extraction plays a major role in any image processing task as it selects only the crucial region consisting of more discriminating features. These discriminating features help in uniquely identifying the thing/object under test. In palm vein recognition task, palm region is the area having complex and wealthy features. Only the palm region is extracted as ROI while eliminating the finger region, and background. Background influence is overcome by applying Otsu thresholding to the input palm vein image as in Han and Lee [19], Kang and Wu [27], Lee [32], Ma et al. [39], Wu et al. [67], and Yan et al. [72].

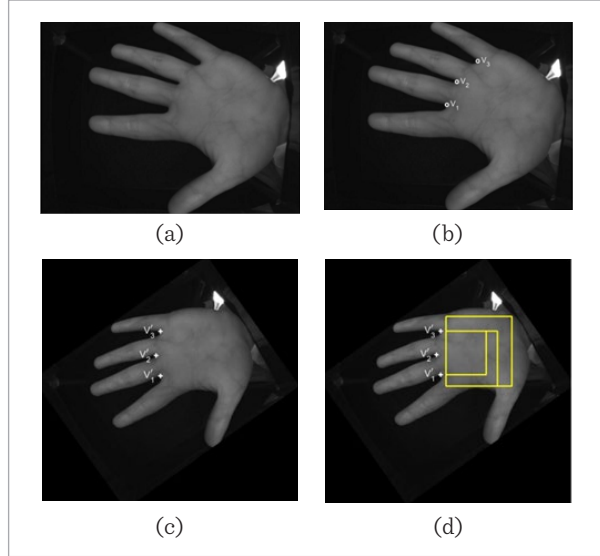
In the resultant binary image, among all the connected regions, the biggest connected region represents the boundary of palm region with fingers, I_B . From this palm region, ROI is extracted with 3-valley point maximal palm extraction strategy. The steps in ROI extraction process are shown in Figure 3. Working of 3-valley point maximal palm extraction strategy: In the input palm vein image, I_{inp} , valley point V_1 lying between index finger & middle finger, V_2 between middle finger & ring finger, and V_3 between ring finger and little finger are located on the palm border based on distance distribution as shown in Figure 3(b).

After locating the 3-valley points, the palm image is aligned, by rotating it by an angle based on its orientation, to overcome the effect of palm rotation during acquisition.

Let the valley points V_1 and V_3 be represented as $V_1(x_1, y_1)$ and $V_3(x_3, y_3)$; θ be the orientation between the line segments $\overline{V_1V_3}$ and a vertical line passing through V_1 . θ is calculated as in Equation (1). Based on the calculated θ value, I_{inp} is rotated by $-\theta$ so as to make $\overline{V_1V_3}$ vertical, resulting in I_{Rot} . Using rotation equation as in Equation (2), the rotated palm boundary points, I_B' in I_{Rot} are computed. In general, any point, P in I_{inp} is mapped to the point, P' in the rotated image I_{Rot} and is computed as in Equation (4). Rotated 3 valley points, V_1', V_2' and V_3' are computed using Equation (4) and are located as shown in Figure 3(c). V_1' and V_3' are moved / translated 20 pixels to the right so that ROI includes only the palm region and not the region from the little finger or index finger. Initially by keeping $\overline{V_1'V_3'}$ as the left edge, a region of 150 pixels width is considered as

Figure 3

ROI extraction process (a) Input palm vein image (b) Locating 3 valley points in the palm boundary (c) Rotating the image according to its orientation (d) Locating maximal ROI



ROI. Then the ROI is grown diagonally in the bottom right direction until all the pixels in the ROI are inside I_B . Then ROI is enlarged along top right direction and right direction to obtain the maximal ROI as shown in Figure 3(d). The maximal ROI, represented by the largest outer yellow rectangle, shown in Figure 3(d) is extracted from I_{Rot} .

The extracted ROI is of varying size depending on the hand size of the person and hand positioning factors during image acquisition. The extracted ROI is normalized to 256 x 256 pixels with bicubic interpolation strategy so as to make the feature extraction and feature matching steps easier.

$$\theta = \tan^{-1} \left(\frac{y_3 - y_1}{x_3 - x_1} \right) \quad (1)$$

$$I'_B = R.(I_B - Center_{old}) + Center_{new}, \quad (2)$$

where, $Center_{old}$ and $Center_{new}$ represent the centers of the images I_{inp} and I_{Rot} respectively. R is the rotation matrix which is defined in Equation (3).

$$R = \begin{vmatrix} \cos(-\theta) & -\sin(-\theta) \\ \sin(-\theta) & \cos(-\theta) \end{vmatrix} \quad (3)$$

$$P' = R.(P - Center_{old}) + Center_{new}. \quad (4)$$

Algorithm 1 defines the steps involved in ROI extraction using 3-valley point maximal palm extraction strategy. Various existing ROI extraction strategies, introduced by Han and Lee [19], Kang and Wu [27], Lee [32], Zhou and Kumar [85] segment the ROI correctly. But the novel 3-valley point maximal palm extraction strategy introduced by the authors in this work segments the palm region easily and correctly and more significantly covers the maximal palm information. In Algorithm 1 given below, the steps 1 – 8, is same as the strategy adopted in our previous work [4]. Let Δ , \sim , δ denote respectively image binarization, image crop, and bicubic interpolation operator. Let c_i , CR , $\#(c)$ represent respectively individual connected region, set of connected regions and number of pixels in region c .

Algorithm 1: ExtractMaximalROI_3ValleyPoints(I_{inp})

Input: Palm vein image, I_{inp}

Output: Segmented ROI, I_{ROI} of size 256 x 256

Threshold $t \leftarrow$ Otsu (I_{inp})

Binarized image $B \leftarrow \Delta(I_{inp}, t)$

Compute $CR \leftarrow \{c_1, c_2, \dots, c_n\}$

$I_B \leftarrow \max(\#(c_i), \forall i = 1..n)$

Locate the valley points V_1, V_2, V_3 using distance distribution

Let V_p be any point with the column same as V_1 .

$\theta \leftarrow$ Angle ($\overline{V_1V_3}, \overline{V_1V_p}$)

$I_{Rot} \leftarrow$ Rotate ($I_{inp}, -\theta$)

$I'_B \leftarrow$ Rotate (I_B)

V'_1, V'_2 and $V'_3 \leftarrow$ Rotate (V_1, V_2, V_3)

Largest area, $Region_{large} \leftarrow$ max (all the rectangular regions with $\overline{V'_1V'_3}$ as their left edge inside I'_B).

$I_{ROI} \leftarrow \sim(Region_{large} \text{ from } I_{Rot})$

$I_{ROI} \leftarrow \delta(I_{ROI}, [256 \ 256])$

3.2. Enhancing the ROI

Palm vein images acquired in contactless mode suffer from blurriness, impulse noise and uneven illumination when compared to contact-based images, stated by Kuamr and Zhou [31] and Yan et al. [72]. These factors affect the performance of the forthcoming feature extraction, feature matching, and decision mak-

ing stages. Enhancing the ROI is carried out normally before performing the extraction of features so as to improve the performance.

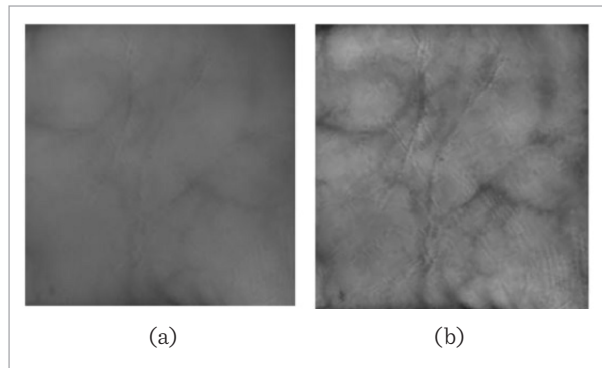
CLAHE does not work on the whole image but work on the smaller regions called tiles or blocks. On each tile, typical histogram equalization is applied. Any noise in the block is not amplified by limiting the contrast of the block. All the adjacent blocks are combined by using bilinear interpolation method to produce the enhanced palm image.

Ma et al. [39] used CLAHE for palm vein image enhancement and improved the recognition result. As CLAHE limits the contrast of the block and does not amplify the noise, in this work, CLAHE is used to increase the contrast of I_{ROI} , shown in Figure 4(a). Contrast enhanced image, I_e is obtained by applying CLAHE over I_{ROI} as in Equation (5) and it is shown in Figure 4(b).

$$I_e = CLAHE(I_{ROI}). \quad (5)$$

Figure 4

Image Enhancement process. (a) Extracted ROI image
(b) CLAHE enhanced ROI



3.3. Extracting the Features

The existence of significant translation, rotation, and scale variations in contactless images require the extracted features to be invariant of such variations. In this work, such invariant features are extracted using SIFT algorithm and Gabor filter, which are discussed in the below subsections.

3.3.1. SIFT Features Extraction

The contactless palm vein images always suffer from translation, scale, orientation, and illumination prob-

lems when compared to contact palm vein images, insisted by Yan et al. [72]. Pan and Kang [48] worked with three local invariant feature extraction methods such as SIFT, Speeded-Up Robust Features (SURF), and Affine-SIFT (ASIFT) in the palm vein images and the result illustrates that the problems existing with contactless palm vein images can be resolved by using these robust invariant feature extraction methods. As palm vein dataset used in this work consists of contactless palm vein images, SIFT, a robust local invariant feature extraction method is adopted. Lowe [38] introduced SIFT features which are invariant to rotation and scale of the image and are robust local features. As these robust features are essential particularly for contactless images, the authors used these features. The variants of SIFT are coloured SIFT (CSIFT) and ASIFT. CSIFT constructs SIFT descriptors in a colour invariant space but which can be used for colour images. Affine-SIFT (ASIFT) simulates a set of sample views of the image by varying the latitude and the longitude angles of the camera, which are not treated by the SIFT method. As the authors use public palm vein dataset which consists of grayscale images, CSIFT is not needed. As the dataset is not custom built, ASIFT is also not needed. Hence the conventional SIFT is used for feature extraction.

SIFT feature extraction includes four steps such as scale-space extrema detection, keypoint localization, orientation assignment, and finding keypoint descriptor and the steps involved in SIFT feature extraction is detailed in Algorithm 2. Let DoG denote difference of Gaussian, D be DoG image, E be extrema, F_p be stable feature points, and F_d be feature descriptors.

Algorithm 2: ExtractSIFTFeatures(I_e)

Input: Enhanced image, I_e of size [256 x 256]

Output: Feature descriptors, F_d with size [930 x 128]

1. $D \leftarrow \text{DoG}(I_e)$
2. $E \leftarrow$ Identify extrema in the scale space
3. $F_p \leftarrow$ locate stable feature points in E
4. Calculate and assign direction $\forall f_p \in F_p$
5. $F_d \leftarrow$ find local feature descriptors of 128 dimension

3.3.2. Gabor Features Extraction

Gabor filter is a powerful texture analysis tool as it resembles the receptive field profiles in the mammalian cortical simple cells. Local texture features are ex-

tracted from the enhanced image, I_e using 2-D Gabor filter as it provides the optimized resolution both in spatial and frequency domain. A circular 2-D Gabor filter is an oriented complex sinusoidal grating which is modulated by a 2-D Gaussian function as in Equation (6).

$$G_{\sigma,u,\theta}(x,y) = g_{\sigma}(x,y).e^{2\pi ju(x\cos\theta+y\sin\theta)}, \quad (6)$$

where, u and θ are respectively, frequency and orientation (in the interval of 0° - 180°) of sinusoidal grating; σ is the standard deviation of the Gaussian envelope; $j = \sqrt{-1}$; $g_{\sigma}(x,y)$ is the Gaussian function which is defined in equation (7).

$$g_{\sigma}(x,y) = \frac{1}{2\pi\sigma^2}.e^{-(x^2+y^2)/(2\sigma^2)}, \quad (7)$$

In the complex form, the 2-D Gabor filter given in Equation (6) is represented as shown in Equation (8).

$$G_{\sigma,u,\theta}(x,y) = R_{\sigma,u,\theta}(x,y) + jI_{\sigma,u,\theta}(x,y) \quad (8)$$

The real and imaginary parts in Equation (8), which are useful in ridge and edge detection respectively, are expressed in Equations (9)-(10).

$$R_{\sigma,u,\theta}(x,y) = g_{\sigma}(x,y).\cos(2\pi u(x\cos\theta + y\sin\theta)) \quad (9)$$

$$I_{\sigma,u,\theta}(x,y) = g_{\sigma}(x,y).\sin(2\pi u(x\cos\theta + y\sin\theta)). \quad (10)$$

The enhanced ROI, I_e is divided into 8×8 non-overlapping subregions of size 32×32 each. In each sub-region, the Gabor parameters such as σ , u and θ are computed as in Ma et al. [39] and the adaptive 2-D Gabor filter is convolved in all the 64 subregions. The real and imaginary parts of the 2-D Gabor filtered image are computed using discrete convolution as mentioned in Eqns. (11-12) while considering a neighbourhood window of size $S \times S$, where $S = 2^* w + 1$.

$$GR_{\sigma,u,\theta}(x,y) = \sum_{i=-w}^w \sum_{j=-w}^w I_e(x+i,y+j).R_{\sigma,u,\theta}(x,y) \quad (11)$$

$$GI_{\sigma,u,\theta}(x,y) = \sum_{i=-w}^w \sum_{j=-w}^w I_e(x+i,y+j).I_{\sigma,u,\theta}(x,y). \quad (12)$$

From the Gabor filtered image, binary vein code feature is extracted in the form of (VC_R, VC_I) as stated in

Equations (13)-(14).

$$VC_R(x,y) = \begin{cases} 1, GR_{\sigma,u,\theta}(x,y) \geq 0 \\ 0, GR_{\sigma,u,\theta}(x,y) < 0 \end{cases} \quad (13)$$

$$VC_I(x,y) = \begin{cases} 1, GI_{\sigma,u,\theta}(x,y) \geq 0 \\ 0, GI_{\sigma,u,\theta}(x,y) < 0 \end{cases} \quad (14)$$

Gabor vein code feature matrices VC_R and VC_I of size 256×256 are obtained by using Equations (13)-(14) with the neighbourhood window of size 3×3 with w being set as 1. In the next module, two different scores are computed by matching the SIFT and Gabor features. Then are ensembled using weighted sum rule and is used in decision making.

3.4. Feature Matching

The extracted SIFT and Gabor features are matched as in the following subsections.

3.4.1. SIFT Feature Matching

Here, in the proposed work, the similarity is computed between two different images based on the cosine of the angle between the SIFT features extracted from those images. The included angle, $\theta_{A,B}$ between the feature vectors A and B is computed as in Equation (15).

$$\theta_{A,B} = \cos^{-1} \left(\frac{A.B}{\|A\| * \|B\|} \right), \quad (15)$$

where, A, B represents the dot product of the vectors A and B , $\|v\|$ represents the norm or length of the vector v and $*$ denotes the scalar multiplication.

When $\theta_{A,B}$ is less than or equal to the threshold value, θ_{thres} , the feature vectors A and B are assumed to be similar. Let the test image be represented by the set of feature vectors F_{tst} and the training image by the feature vectors F_{trn} , both are of size $nrows \times ncols$.

The number of matching features between F_{tst} and F_{trn} is calculated as stated in Algorithm 3. The included angles, θ_j , $J = 1 \dots \#$ (SIFT descriptors of F_{trn}), between the first SIFT descriptor of F_{tst} and all the individual SIFT descriptors of F_{trn} are computed. Let θ_t , $t \in J$, be minimum value in the set of angles θ_j . If θ_t is less than or equal to θ_{thres} , then the t^{th} feature vector of F_{trn} is the closely matching feature to the currently testing feature. As this t^{th} feature of F_{trn} is now matched

to the current feature of F_{tst} it is removed from F_{trn} . If the minimum of θ_j is greater than θ_{thres} , it depicts that for the currently testing feature, there is no matching feature. Then the included angles between second SIFT descriptor of F_{tst} and all the available individual SIFT descriptors of F_{trn} is computed and the above mentioned process is repeated until the last feature of F_{tst} . Number of matching features, $Matchcnt$, between F_{tst} and F_{trn} is calculated as in Equation (16).

$$Matchcnt = nrows - |F_{trn}|, \quad (16)$$

where $|F_{trn}|$ denotes number of unmatched features of training image i.e., number of rows in F_{trn} that remain at the end of feature matching.

Algorithm 3: ComputeMatchCount(F_{tst} , F_{trn})

Input: F_{tst} , F_{trn} are feature matrices of testing and training images respectively. Both are of size $nrows \times ncols$.

Output: $Matchcnt$ – number of matching features between F_{tst} and F_{trn}

```

begin
  for  $i = 1$  to  $nrows$  do
    begin
       $f_1 \leftarrow F_{tst}(i, :)$  // select  $i^{th}$  feature i.e.,  $i^{th}$  row of  $F_{tst}$ 
       $\theta_j = []$ 
      for  $j = 1$  to  $|F_{trn}|$  do
        begin
           $f_2 \leftarrow F_{trn}(j, :)$ 
           $\theta_j = [\theta_j, \theta_{f_1, f_2}]$ 
        end for
       $\theta_t \leftarrow \min(\theta_j)$  where  $1 \leq t \leq |F_{trn}|$ 
      if  $(\theta_t \leq \theta_{thres})$ 
        begin
           $f_t \leftarrow F_{trn}(t, :)$ 
           $F_{trn} \leftarrow \Theta(F_{trn}, f_t)$  //  $\Theta$  - set difference operator
        end if
      end for
       $Matchcnt = nrows - |F_{trn}|$ 
    return  $Matchcnt$ 
  end

```

3.4.2. Gabor Feature Matching

Han and Lee [19], Lee [32], and Ma et al. [39] used normalized Hamming distance measure (NHD) for similarity measurement between training and testing veincode features. As NHD provides translation and rotation invariance, in this work, NHD is used for similarity calculation over the multiresolution Gabor features.

Let X and Y be the training and testing veincode feature matrix respectively. The normalized Hamming distance is defined as in Equation (17).

$$NHD = \frac{\sum_{i=\max(1,1+s)}^{i=\min(N,N+s)} \sum_{j=\max(1,1+t)}^{j=\min(N,N+t)} (X_R(i+s, j+t) \otimes Y_R(i, j)) + (X_I(i+s, j+t) \otimes Y_I(i, j))}{2H(s)H(t)} \quad (17)$$

Here, X_R and Y_R are the real part veincode features of X and Y respectively, whereas X_I and Y_I represent imaginary part of veincode features; \otimes is the exclusive-OR operator; $N \times N$ is the size of the veincode feature matrix; s and t represent translation along horizontal and vertical directions; $H(m)$ is calculated as in Equation (18).

$$H(m) = \min(N, N + m) - \max(1, 1 + m). \quad (18)$$

To insist translation and rotation invariance, NHD is computed for all the possible values of $s \in \{1, 2, \dots, 8\}$ and $t \in \{1, 2, \dots, 8\}$. Out of all these NHDs, the minimum value is considered as the distance between X and Y .

3.5. Decision Making

SIFT features extracted from test image are compared against SIFT features of training images using *ComputeMatchCount* algorithm and $Matchcnt$, which denotes the number of matching SIFT features between any two images (training and testing) is computed. Higher the value of $Matchcnt$, the more similar the images are. Normalizing the $Matchcnt$ values is essential, and they are normalized using min-max normalization method.

Let $nmatches$ denote a vector of number of matching features ($Matchcnt$) between a test image and all the individual template images. The score from SIFT features matching, S_s is computed by employing min-max normalization to $nmatches$ as in Equation (19) so that the score is normalized to the range of 0 to 1.

$$S_{s_i} = \frac{nmatches - \min(nmatches)}{\max(nmatches) - \min(nmatches)}, \quad (19)$$

where S_s and $nmatches$ are the vectors of length equal to the number of training samples. S_{s_i} and $nmatches_i$ denote the i^{th} element of the corresponding vectors.

Normalized Hamming distance which is computed between Gabor features of test image and training images lie in the range of 0 to 1. NHD is a dissimilarity measure whereas S_s is the similarity score from SIFT features. The similarity score from Gabor features, S_g , is computed as in Equation (20), by subtracting all the NHD values from 1.

$$S_{g_i} = 1 - V_{NHD_i}, \quad (20)$$

where, S_g and the normalized Hamming distance vector, V_{NHD} , are the vectors of length equal to the number of training samples. S_{g_i} and V_{NHD_i} denote the i^{th} element of the corresponding vectors.

The two similarity scores computed from SIFT and Gabor features are ensembled using weighted sum rule to compute the final score, S_f . Let α and β denote the weightages assigned to the individual scores. The weighted sum rule in Equation (21) represents the ensembling of scores.

$$S_f = \alpha.S_s + \beta.S_g. \quad (21)$$

The computed final score, S_f is used in identification. For a test image, this final matching score is computed with all the training images. The maximum of these scores, if it is greater than the preset matching threshold, the test image is identified as the class label corresponding to the training image with highest score.

4. Experimental Results

Experiments were conducted on CASIA multispectral palmprint image database V1.0 [9] and VERA palm vein database [60]. A detailed description of these data sets was provided in our previous work, Ananthi et al. [4].

4.1. Performance Metrics

For both authentication and identification of the claimant, matching score threshold, S_{thres} is set.

During authentication or verification, the claimant's palm vein image is compared against his/her own templates only. If S_f computed between the test image and the claimant's templates is greater than or equal to S_{thres} , then the claimant is declared as genuine otherwise as imposter as in Equation (22).

$$Decision = \begin{cases} Genuine, S_f \geq S_{thres} \\ Im\ poster, otherwise \end{cases}, \quad (22)$$

where S_f is the score computed between the test image and the claimant's template.

In the identification process, the claimant is identified who he/she is. Computation of matching scores between the test image and all the registered templates is carried out. Let the result be $MScores$. If maximum of $MScores$ corresponds to i^{th} person, the test image is identified as i^{th} person as in Equation (23).

$$Class = i, \text{ if } \max(MScores) = MScores[i] \ \& \ MScores[i] > S_{thres}. \quad (23)$$

Consider the below example for identification. Suppose two samples are trained per subject / class and the $MScores$ vector contains the values as specified here.

1	2	3	4	...	128	129	...
0.231	0.957	0.897	0.983	...	0.996	0.998	...

The values above the vector represent the position. As two samples are trained per class, the values in positions 1 and 2 correspond to class 1, positions 3 and 4 correspond to class 2, and so on. Now the test image is identified as class 65 since 0.998 is the largest value and is above the preset matching threshold, 0.91.

Correct recognition result (CRR), false acceptance rate (FAR), false rejection rate (FRR), equal error rate (EER), and identification time are computed as the performance metrics. CRR is the ratio of number of images identified correctly to the total number of images tested and is computed as in Equation (24).

$$CRR = \frac{\# \text{ samples correctly identified}}{\# \text{ samples tested}} \times 100. \quad (24)$$

FAR is the ratio of number of imposter images being accepted as genuine to the total number of images tested and is computed as in Equation (25).

$$FAR = \frac{\# \text{ wrongly accepted imposter images}}{\# \text{ samples tested}} \times 100. \quad (25)$$

FRR is the ratio of number of genuine images being rejected as imposter to the total number of images tested and is computed as in Equation (26).

$$FRR = \frac{\# \text{wrongly rejected genuine images}}{\# \text{samples tested}} \times 100. \quad (26)$$

EER is equal to FAR at some threshold, S_{thres} , where both FAR and FRR are equal, i.e., $FAR_{S_{thres}} = FRR_{S_{thres}}$, where $FAR_{S_{thres}}$ and $FRR_{S_{thres}}$ are FAR and FRR computed at the threshold, S_{thres} . EER is computed by plotting a receiver operating characteristics (ROC) curve which is a graphical curve drawn FAR vs. FRR for fifteen different values of S_{thres} ranging from 0.5 to 0.95.

4.2. Performance Evaluation

In the proposed work, the right hand palm images of both the databases are used. Table 1 shows the performance of the system with CASIA database, considering various values for matching threshold, θ_{thres} over the SIFT features. From table 1, it is understood that the optimal value for θ_{thres} is 20° .

Table 1

Selection of optimal matching angle for SIFT features

# train per subject	# test per subject	EER (in %) with θ_{thres}				
		10°	15°	20°	25°	30°
2	4	0.052	0.042	0.036	0.048	0.057
3	3	0.45	0.039	0.031	0.035	0.042
4	2	0.036	0.029	0.026	0.032	0.039
5	1	0.038	0.035	0.031	0.037	0.043

With exhaustive experimentation, the empirically chosen value for preset matching threshold is 0.91 for both authentication and identification tasks.

Exhaustive experiments are conducted with three different test cases in the CASIA database. Test case 1 involves 850 nm right hand palm images as in Zhou and Kumar [85] whereas test case 2 uses 940 nm right palm images for experimentation. Test case 3 uses a total of 1200 right palm images acquired at both 850 nm and 940 nm wavelengths. In the VERA palm vein database, a total of 1100 right palm images are used for experimentation.

In the input palm vein image, after applying Otsu thresholding, ROI of size 256 x 256 is extracted by 3-valley point maximal palm extraction method. The extracted ROI is then enhanced using contrast limited adaptive histogram equalization method. SIFT features and adaptive Gabor features are extracted from the enhanced ROI. Each ROI results in 930 number of 128-dimension SIFT features and Gabor vein code feature matrices VC_R and VC_I of size 256 x 256.

4.2.1. Performance Evaluation with CASIA Database

Test cases 1 & 2 use only 600 images. Suppose that only 50% of the images are tested. Then in test cases 1 & 2, only 300 images are tested, which is not sufficient to report the system performance. As a result, it is proposed to work with different combinations of training and testing in all the test cases so as to improve the test set size. While testing two samples per subject, various combination of samples tested are $\{(1, 2), (1, 3), (1, 4), (1, 5), (1, 6), (2, 3), (2, 4), (2, 5), (2, 6), (3, 4), (3, 5), (3, 6), (4, 5), (4, 6), (5, 6)\}$, leading to a total of 15 ($6C_2$) combinations. When the samples 1 and 2 of each subject are tested, the remaining samples, 3, 4, 5 and 6 of each subject are trained. While testing the samples 1 and 2, totally 200 (100 subjects x 2 samples) samples are tested. For 15 such combinations, a total of 3000 (15 combinations x 200 samples) samples are tested. Similarly, it is done for other possible combinations.

Table 2 shows the system performance in terms of EER for test cases 1 and 2. For various training and testing combinations, EER is listed. In Table 2, the bolded items represent the optimal EER obtained in both the test cases. From this table, it is inferred that while training 4 out of 6 samples per subject, increased system performance is achieved.

Table 3 shows the performance of the system in test case 3. In test case 3, the best performance is achieved while training 8 samples per subject and testing the remaining 4 samples per subject. In Table 3, the bolded data, 0.026%, denotes the best EER obtained in test case 3. From tables 2 & 3 it is evident that the ensemble score results in better EER when compared to using only the individual scores.

Table 4 exhibits the system performance with all the three test cases for various combination of weighting parameters, α and β . From Table 4, it is clear

Table 2

System performance of test cases 1 & 2 with CASIA database

# train per subject	# test per subject	# of combinations	Total images trained	Total images tested	EER (in %) in with					
					Test case 1			Test case 2		
					S_s score	S_g score	Ensembled score, S_F	S_s score	S_g score	Ensembled score, S_F
2	4	15	3000	6000	0.051	0.049	0.046	0.049	0.039	0.036
3	3	20	6000	6000	0.045	0.039	0.032	0.037	0.034	0.031
4	2	15	6000	3000	0.042	0.034	0.029	0.035	0.031	0.026
5	1	6	3000	600	0.049	0.036	0.033	0.043	0.037	0.031

Table 3

System performance of test case 3 with CASIA database

# train per subject	# test per subject	# of combinations	Total images trained	Total images tested	EER (in %) in Test case 3 with		
					S_s score	S_g score	Ensembled score, S_F
4	8	495	198000	396000	0.093	0.085	0.076
5	7	792	396000	554400	0.089	0.072	0.065
6	6	924	554400	554400	0.052	0.048	0.037
7	5	792	554400	396000	0.034	0.032	0.030
8	4	495	396000	198000	0.032	0.029	0.026
9	3	220	198000	66000	0.041	0.032	0.034

Table 4Deciding the suitable weight parameters for α and β

α	β	EER (%) in Test case		
		1	2	3
0.1	0.9	0.081	0.078	0.092
0.2	0.8	0.063	0.059	0.078
0.3	0.7	0.035	0.040	0.061
0.4	0.6	0.029	0.026*	0.026*
0.5	0.5	0.031	0.027	0.032
0.6	0.4	0.039	0.034	0.43
0.7	0.3	0.059	0.049	0.053
0.8	0.2	0.068	0.051	0.064
0.9	0.1	0.074	0.072	0.077

* denotes the optimal EER achieved with CASIA database.

that the weight combination (0.4, 0.6) for α and β outperforms.

Table 5 compares the proposed work with the state-of-art methods for CASIA palm vein database. From Table 5, it is understood that the proposed method works well when compared to the state-of-art methods. Authors' previous work, Ananthi et al. [4] results in better EER when compared to the proposed work as it used the Curvelet multiresolution transform. Though the proposed work uses SIFT and Gabor features, it is better comparable to Haar wavelet decomposition and partial least squares method, introduced by Wu et al. [68]. As the authors' previous work [4] resulted in FAR of 0.01%, it can be used in applications like finance transaction where imposter acceptance is highly prohibited. Proposed work can be deployed in applications where the genuine person should not be rejected as imposter. An example application is

Table 5

Comparison with the state-of-art methods for CASIA palm vein database through EER

Authors	Methods used	Year	EER (in %)
Zhou et al. [85]	Neighborhood matching Radon transform and Hessian-phase-based approach	2011	0.32 # 0.66 **
Kang et al. [27]	Principal curvature, Mutual foreground – Local Binary Pattern	2014	0.267
Yan et al. [72]	SIFT features, multi-sampling, and feature-level fusion	2015	0.16
Ma et al. [39]	Adaptive Gabor filter	2017	0.12
Wu et al. [68]	Haar wavelet decomposition and partial least squares algorithm	2019	0.0292
Ananthi et al. [4]	Curvelet features with score level fusion	2021	0.021
Proposed work	SIFT and Gabor features with score ensembling	2022	0.026

- EER with left palm images, ** - EER with right palm images

authenticating the regular customers for discount offers in large retail shops. Through the ROC curves, the state-of-art methods are compared in Figure 5. The ROC curve which comes close to the origin represents the best EER. Figure 5 proves that the proposed system works better than the state-of-methods. The proposed method is compared with the state-of-art methods using identification time in Table 6. The proposed method is better comparable to Yan et al. [72]. Identification time of the proposed work is comparatively larger than the authors' previous work [4] as SIFT feature extraction and matching takes ade-

Figure 5

Performance comparison with the start-of-art methods for CASIA database using ROC curve

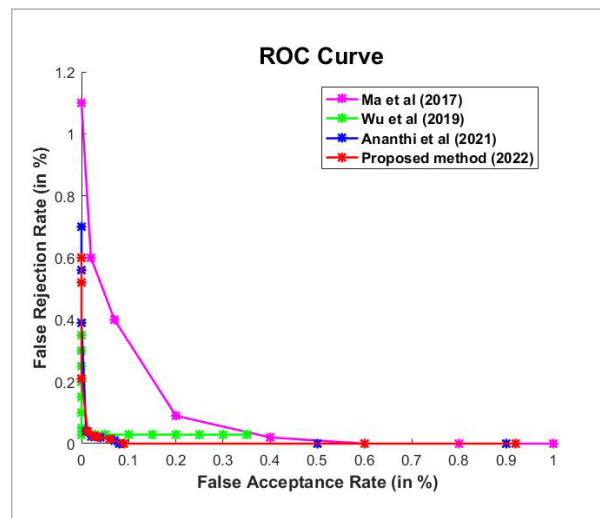


Table 6

Comparison with the state-of-art methods for CASIA palm vein database through identification time

Authors	Methods used	Year	Identifica-tion time (in sec)
Kang et al. [27]	Principal curvature, Mutual foreground – Local Binary Pattern	2014	4.58
Yan et al. [72]	SIFT features, multi-sampling, and feature-level fusion	2015	3.25
Ma et al. [39]	Adaptive Gabor filter	2017	2.44
Wu et al. [68]	Haar wavelet decomposition & partial least squares algorithm	2019	0.7299
Ananthi et al. [4]	Curvelet features with score level fusion	2021	0.09
Proposed work	SIFT and Gabor features with score ensembling	2022	0.675

quate time. As the identification time of the proposed work is less than a second, it can better be used in the real-time palm vein identification applications. Time complexity for authentication and identification are respectively $O(m)$ and $O(nm)$ where m is the number of features and n is the number of templates compared. The proposed work resulted in the recognition rate of 99.73% for CASIA palm vein database.

4.2.2. Performance Evaluation with VERA Database

A total of 1100 right palm images acquired from 110 subjects of Vera database are used for evaluating the performance of the proposed system. As with CASIA database, for various combinations of training and testing samples, the system performance is evaluated for Vera database and is shown in Table 7. From Table 7, it is evident that, for the (training, testing) combination (7, 3) the proposed system outperforms. System performance with Vera database is compared with the state-of-art methods in Table 8 and this table shows that the proposed method is superior in performance and yields comparable improvement to Hernández-García et al. [21]. Comparison of system performance with the state-of-art methods for VERA palm vein database using ROC curve is shown in Figure 6. A recognition rate of 99.89% was achieved with VERA palm vein database.

Figure 6

Performance comparison with the start-of-art methods for VERA database using ROC curve

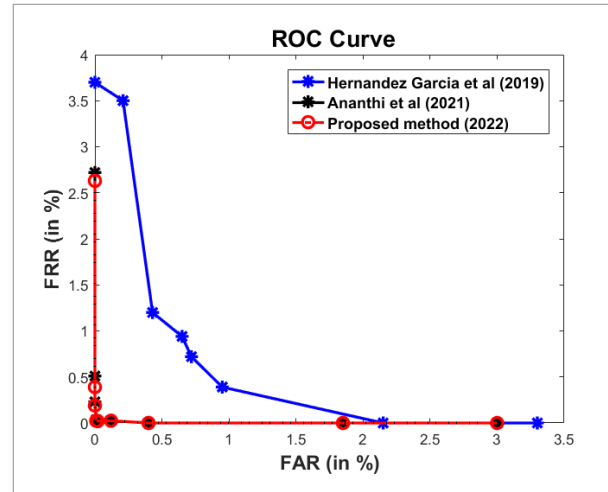


Table 7

System performance with VERA database

# train per subject	# test per subject	# of combinations	Total images trained	Total images tested	EER (in %)
5	5	252	138600	138600	0.3186
6	4	210	138600	92400	0.1086
7	3	120	92400	39600	0.0205
8	2	45	39600	9900	0.0310

Table 8

Proposed method comparison with state-of-art methods for VERA database

Authors	Method	Year	EER (in %)
Tome et al. [60]	Local Binary Pattern (LBP) and histogram intersection metric	2015	3.75
Hernández-García et al. [21]	Coarse-to-fine Patch Match algorithm with Daisy descriptor and Displacement uniformity texture	2019	0.72
Ahmad et al. [1]	Wave atom transform	2020	3.61
Ananthi et al. [4]	Curvelet features with score level fusion	2021	0.0207
Proposed work	SIFT and Gabor features with score ensembling	2022	0.0205

5. Conclusion

In the proposed work, human identification was achieved with the palm vein trait. Experimentation was done with CASIA multispectral palm print im-

age database V 1.0 and VERA palm vein database. The novel palm region extraction strategy, 3-valley point strategy, segments the maximal possible palm

from the input palm vein image. The segmented ROI is enhanced with CLAHE, a powerful image enhancement technique. As the dataset consists of contactless images, it is more prone to scale and rotation changes. Scale invariant features are extracted with SIFT and multiresolution features with Gabor filter. Separate scores are computed for both types of features and they are ensembled using weighted sum rule. The performance of the system while using the ensembled score is better than using a single score. As the time complexity is linear for the proposed system, it can be used in the real-time authentication applications.

References

1. Ahmad, F., Lee-Ming, C., Asif, K. Lightweight and Privacy-Preserving Template Generation for Palm-Vein-Based Human Recognition. *IEEE Transactions on Information Forensics and Security*, 2020, 5, 184-194. <https://doi.org/10.1109/TIFS.2019.2917156>
2. Al-Juboori, A. M., Bu, W., Wu, X., Zhao, Q. Palm Vein Verification Using Multiple Features and Locality Preserving Projections. *The Scientific World Journal*, 2014, 2014, 1-11, <https://doi.org/10.1155/2014/246083>
3. Al-Zubi, R. T., Darabkh, K. A., Jararweh, Y. I. A Powerful Yet Efficient Iris Recognition Based on Local Binary Quantization. *Information Technology and Control*, 2014, 43(3), 244-251. <https://doi.org/10.5755/j01.itc.43.3.5225>
4. Ananthi, G., Sekar, J. R., Arivazhagan, S. Human Palm Vein Authentication Using Curvelet Multiresolution Features and Score Level Fusion. *Visual Computer*, 2021, <https://doi.org/10.1007/s00371-021-02253-9>
5. Arakala, A., Davis, S. A., Hao, H., Horadam, K. J. Value of Graph Topology in Vascular Biometrics. *IET Biometrics*, 2016, 6(2), 117-125. <https://doi.org/10.1049/iet-bmt.2016.0073>
6. Arivazhagan, S., Ganesan, L., Srividya, T. Iris Recognition Using Multi-Resolution Transforms. *International Journal of Biometrics*, 2009, 1(3), 254-267, <https://doi.org/10.1504/IJBM.2009.024273>
7. Babalola, F. O., Bitirim, Y., Toygar, Ö. Palm vein Recognition Through Fusion of Texture-based and CNN-Based Methods. *Signal, Image and Video Processing*, 2020, 15, 459-466, <https://doi.org/10.1007/s11760-020-01765-6>
8. Balasubramanian, C., Raja Sekar, J. An Integrated Methods for Refined Facial-Image Retrieval Using Sift and Click-Through Data. *International Journal of Engineering and Advanced Technology*, 2019, 9(1S6), 48-51, <https://doi.org/10.35940/ijeat.A1011.1291S619>
9. CASIA-Multispectral-Palmprint V1 dataset, <http://biometrics.idealtest.org/>. Accessed on June 07, 2016.
10. Chen, P., Ding, B., Wang, H., Liang, R., Zhang, Y., Zhu, W., Liu, Y. Design of Low-Cost Personal Identification System That Uses Combined Palm Vein and Palmprint Biometric Features. *IEEE Access*, 2019, 7, 15922-15931, <https://doi.org/10.1109/ACCESS.2019.2894393>
11. Chengathir Selvi, M., Muneeswaran, K. Unconstrained Face Recognition in Surveillance Videos Using Moment Invariants. *International Journal of Biomedical Engineering and Technology*, 2017, 25(2-4), 282-299. <https://doi.org/10.1504/IJBET.2017.087729>
12. Cho, S., Oh, B-S., Kim, D., Toh, K-A. Palm-Vein Verification Using Images from the Visible Spectrum. *IEEE Access*, 2021, 9, 86914-86927, <https://doi.org/10.1109/ACCESS.2021.3089484>
13. Cross, J.M., Smith C.L. Thermographic Imaging of Subcutaneous Vascular Network of the Back of the Hand for Biometric Identification. *Proceedings of IEEE 29th International Carnahan Conference on Security Technology (ICCST)*, Sanderstead, Surrey, England, 1995, 20-35.
14. Deepamalar, M., Madheswaran, M. An Improved Multimodal Palm Vein Recognition System Using Shape and Texture Features. *International Journal of Computer Theory and Engineering*, 2010, 2(3), 436-444, <https://doi.org/10.7763/ijcte.2010.v2.182>. <https://doi.org/10.7763/IJCTE.2010.V2.182>
15. Elnasir, S., Shamsuddin, S.M., Farokhi, S. Accurate Palm Vein Recognition Based on Wavelet Scattering

Acknowledgement

The authors thank Chinese Academy of Sciences' Institute of Automation and Idiap Research Institute, Martigny, Switzerland for providing the CASIA-MS-Palmprint V1.0 and VERA Palm vein database respectively.

Declarations

Funding: Not applicable

Conflicts of interest / Competing interests: The authors do not have any conflict of interest

Availability of data and material: Not applicable

Code availability: Not applicable

- and Spectral Regression Kernel Discriminant Analysis. *Journal of Electronic Imaging*, 2015, 24(1), 1-14, <https://doi.org/10.1117/1.JEI.24.1.013031>
16. Greitans, M., Pudzs, M., Fuksis, R. Palm Vein Biometrics Based on Infrared Imaging and Complex Matched Filtering. *Proceedings of ACM SIGMM Multimedia and Security Workshop, Rome, 2010*, 101-106. <https://doi.org/10.1145/1854229.1854250>
 17. Gupta, P., Gupta, P. Multi-modal Fusion of Palm-Dorsa Vein Pattern for Accurate Personal Authentication. *Knowledge Based Systems*, 2015, 81(C) 117-130. <https://doi.org/10.1016/j.knosys.2015.03.007>
 18. Gupta, P., Gupta, P. Slap Fingerprint Segmentation Using Symmetric Filters Based Quality. *Proceedings of International Conference on Advances in Pattern Recognition (ICAPR), Kolkata, 2015*, 1-6. <https://doi.org/10.1109/ICAPR.2015.7050688>
 19. Han, W., Lee, J. Palm Vein Recognition Using Adaptive Gabor Filter. *Expert Systems with Applications*, 2012, 39(18), 13225-13234, <https://doi.org/10.1016/j.eswa.2012.05.079>
 20. Hawkes, P.L., Clayden, D.O. Veincheck Research for Automatic Identification of People. *Hand and Fingerprint Seminar, NPL, 1993*, 230-236.
 21. Hernández-García, R., Barrientos, R. J., Rojas, C., Mora, M. Individuals Identification Based on Palm Vein Matching under a Parallel Environment. *Applied Sciences*, 2019, 9(14), 2805. <https://doi.org/10.3390/app9142805>
 22. Jain, A. K., Bolle, R., Pankanti, S. *Biometrics Personal Identification in Networked Society*. US, Springer-Verlag, 2006.
 23. Jia, W., Gao, J., Xia, W., Zhao, Y., Min, H., Lu, J-T. A Performance Evaluation of Classic Convolutional Neural Networks for 2D and 3D Palmprint and Palm Vein Recognition. *International Journal of Automation and Computing*, 2021, 18(1), 18-44. <https://doi.org/10.1007/s11633-020-1257-9>
 24. Joardar, S., Chatterjee, A., Rakshit, A. A Real-Time Palm Dorsa Subcutaneous Vein Pattern Recognition System Using Collaborative Representation-Based Classification. *IEEE Transaction and Instrumentation Measurements*, 2015, 64(4), 959-966. <https://doi.org/10.1109/TIM.2014.2374713>
 25. Joardar, S., Chatterjee, A., Rakshit, A. Real-Time NIR Imaging of Palm Dorsa Subcutaneous Vein Pattern Based Biometrics: An SRC Based Approach. *IEEE Instrumentation and Measurements Magazine*, 2016, 19(2), 13-19. <https://doi.org/10.1109/MIM.2016.7462787>
 26. Kang, W., Liu, Y., Wu, Q., Yue, X. Contact-Free Palm-Vein Recognition Based on Local Invariant Features. *PLoS ONE*, 2014, 9(5), 1-12. <https://doi.org/10.1371/journal.pone.0097548>
 27. Kang, W., Wu, Q. Contactless Palm Vein Recognition Using a Mutual Foreground-Based Local Binary Pattern. *IEEE Transactions on Information Forensics and Security*, 2014, 9(11), 1974-1985. <https://doi.org/10.1109/TIFS.2014.2361020>
 28. Kilian, V., Ally, N., Nombo, J., Abdalla, A.T., Maiseli, B. Cost-effective and Accurate Palm Vein Recognition System Based on Multiframe Super-Resolution Algorithms. *IET Biometrics*, 2020, 9(3), 118-125, <https://doi.org/10.1049/iet-bmt.2019.0016>
 29. Kong, A. W. K., Zhang, D. Competitive Coding Scheme for Palmprint Verification. *Proceedings of International Conference on Pattern Recognition (ICPR 2004)*, IEEE, Cambridge, UK, 2004, 520-523. <https://doi.org/10.1109/ICPR.2004.1334184>
 30. Kumar, A., Venkata Prathyusha, K. Personal Authentication Using Hand Vein Triangulation and Knuckle Shape. *IEEE Transaction on Image Processing*, 2009, 18(9), 2127-2136. <https://doi.org/10.1109/TIP.2009.2023153>
 31. Kumar, A., Zhou, Y. Contactless Fingerprint Identification Using Level Zero Features. *Proceedings of IEEE Computer Vision and Pattern Recognition Workshops (CVPR Workshops), Colorado Springs, CO, 2011*, 114-119. <https://doi.org/10.1109/CVPRW.2011.5981823>
 32. Lee, J. A Novel Biometric System Based on Palm Vein Image. *Pattern Recognition Letters*, 2012, 33(12), 1520-1528, <https://doi.org/10.1016/j.patrec.2012.04.007>
 33. Lee, Y-P. Palm Vein Recognition Based on a Modified (2D)2 LDA. *Signal Image Video Processing*, 2015, 9(1), 229-242, <https://doi.org/10.1007/s11760-013-0425-6>
 34. Li, Q., Zeng, Y., Peng, X., Yang, K. Curvelet-based Palm Vein Biometric Recognition. *Chinese Optics Letters*, 2010, 8(6), 577-579. <https://doi.org/10.3788/COL20100806.0577>
 35. Li, Q., Zeng, Y., Yang, K. Wavelet-based Palm Vein Recognition System. *Journal of Innovative Optical Health Sciences*, 2010, 3(2), 131-134. <https://doi.org/10.1142/S1793545810000940>
 36. Li, Q., Li, X., Guo, Z., You, J. Online Personal Verification by Palmvein Image Through Palmprint-Like and Palmvein Information. *Neurocomputing*, 2015, 147, 364-371. <https://doi.org/10.1016/j.neucom.2014.06.050>
 37. Lin, C. L., Fan, K.C. Biometric Verification Using Thermal Images of Palm-Dorsa Vein Patterns. *IEEE Transactions on Circuits and Systems for Video Technology*, 2004, 14(2), 199-213. <https://doi.org/10.1109/TCSVT.2003.821975>

38. Lowe, D.G. Distinctive Image Features from Scale-Invariant Keypoints. *International Journal of Computer Vision*, 2004, 60(2), 91-110. <https://doi.org/10.1023/B:VISI.0000029664.99615.94>
39. Ma, X., Jing, X., Huang, H., Cui, Y., Mu, J. Palm Vein Recognition Scheme Based on an Adaptive Gabor filter. *IET Biometrics*, 2017, 6(5), 325-333. <https://doi.org/10.1049/iet-bmt.2016.0085>
40. MacGregor, P., Welford, R. Veincheck: Imaging for Security and Personnel Identification. *Advanced Imaging*, 1991, 6(7), 52-56.
41. Masaki Watanabe, T. E., Shiohara, M., Sasaki, S. Palm Vein Authentication Technology and Its Applications. *Proceedings of Biometric Consortium Conference (BC 2005)*, Hyatt Regency Crystal City, Arlington, VA, USA, 2005, 1-2.
42. Michael, G. K. O., Connie, T., Jin, A. T. B. Design and Implementation of a Contactless Palm Print and Palm Vein Sensor. *Proceedings of Eleventh International Conference on Control, Automation, Robotics and Vision*, 2010, 1268-1273. <https://doi.org/10.1109/ICARCV.2010.5707951>
43. Mirmohamadsadeghi, L., Drygajlo, A. Palm Vein Recognition with Local Texture Patterns. *IET Biometrics*, 2014, 3(4), 198-206. <https://doi.org/10.1049/iet-bmt.2013.0041>
44. Mirmohamadsadeghi, L., Drygajlo, A. Palm vein Recognition with Local Binary Patterns and Local Derivative Patterns. *Proceedings of IEEE International Joint Conference on Biometrics*, 2011, 1-6. <https://doi.org/10.1109/IJCB.2011.6117804>
45. Moravec, J. Hand Contour Classification Using Differential Evolution Algorithm with Ensemble of Parameters and Mutation and Crossover. *Information Technology and Control*, 2020, 49(1), 55-79. <https://doi.org/10.5755/j01.itc.49.1.24140>
46. Muneeswaran, K., Ganesan, L., Arumugam, S., Ruba Soundar, K. Texture Classification with Combined Rotation and Scale Invariant Wavelet Features. *Pattern recognition*, 2005, 38(10), 1495-1506. <https://doi.org/10.1016/j.patcog.2005.03.021>
47. Obayya, M. I., El-Ghandour, M., Alrowais, F. Contactless Palm Vein Authentication Using Deep Learning With Bayesian Optimization. *IEEE Access*, 2021, 9, 1940-1957. <https://doi.org/10.1109/ACCESS.2020.3045424>
48. Pan, M., Kang, W. Palm Vein Recognition Based on Three Local Invariant Feature Extraction Algorithms. *Lecture Notes in Computer Science (Including Subseries Lecture Notes in Artificial Intelligence and Lecture Notes in Bioinformatics)*, 7098 LNCS, 2011, 116-124. https://doi.org/10.1007/978-3-642-25449-9_15
49. Pan, Z., Wang, J., Shen, Z., Chen, X., Li, M. Multi-layer Convolutional Features Concatenation with Semantic Feature Selector for Vein Recognition. *IEEE Access*, 2019, 7, 90608-90619. <https://doi.org/10.1109/ACCESS.2019.2927230>
50. Phalguni. A Step Towards Development of Aid For Visually Challenged. *Sadhana*, 2017, 42(2), 187-192. <https://doi.org/10.1007/s12046-017-0591-2>
51. Piciuccio, E., Maiorana, E., Campisi, P. Palm Vein Recognition Using a High Dynamic Range Approach. *IET Biometrics*, 2018, 7(5), 439-446. <https://doi.org/10.1049/iet-bmt.2017.0192>
52. Qin, H., El-Yacoubi, M.A., Li, Y., Liu, C. Multi-Scale and Multi-Direction GAN for CNN-Based Single Palm-Vein Identification. *IEEE Transactions on Information Forensics and Security*, 2021, 16, 2652-2666. <https://doi.org/10.1109/TIFS.2021.3059340>
53. Qiu, S., Liu, Y., Zhou, Y., Huang, J., Nie, Y. Finger-vein Recognition Based on Dual-Sliding Window Localization And Pseudo-Elliptical Transformer. *Expert Systems with Applications*, 2016, 64(C), 618-632. <https://doi.org/10.1016/j.eswa.2016.08.031>
54. Raja Sekar, J., Arivazhagan, S., Shobana Priyadarshini, S., Shunmugapriya, S. Iris recognition Using Combined Statistical and Co-occurrence Multi-resolutional Features. *International Journal of Pattern Recognition and Artificial Intelligence*, 2013, 27(01), 1356001. <https://doi.org/10.1142/S0218001413560016>
55. Stanuch, M., Wodzinski, M., Skalski, A. Contact-free Multispectral Identity Verification System Using Palm Veins and Deep Neural Network. *Sensors*, 2020, 20(19), 1-17. <https://doi.org/10.3390/s20195695>
56. Su, C. L. Palm Extraction and Identification. *Expert Systems with Applications*, 2009, 36(2), 1082-1091. <https://doi.org/10.1016/j.eswa.2007.11.001>
57. Sun, J., Abdulla, W. Palm Vein Recognition by Combining Curvelet Transform and Gabor Filter. *Proceedings of Eighth China Biometric Conference (CCBR2013)*, Springer International Publishing, Jinan, China, 2013, 1-8. https://doi.org/10.1007/978-3-319-02961-0_39
58. Thillainayagi, R., Senthil Kumar, K. Hybrid Bi-dimensional Empirical Mode Decomposition Based Enhancement Technique for Extreme Low Contrast UAV

- Thermal Images. *Sadhana*, 2019, 44, 146-156. <https://doi.org/10.1007/s12046-019-1130-0>
59. Toh, K., Eng, H., Choo, Y. Identity Verification Through Palm Vein and Crease Texture. *Advances in Biometrics*, 2006, 546-553. https://doi.org/10.1007/11608288_73
 60. Tome, P., Marcel, S. On the Vulnerability of Palm Vein Recognition to Spoofing Attacks. *Proceedings of International Conference on Biometrics (ICB)*, Phuket, Thailand, 2015, 319-325. <https://doi.org/10.1109/ICB.2015.7139056>
 61. Wang, F., Han, J. Robust Multimodal Biometric Authentication Integrating Iris, Face and Palmprint. *Information Technology and Control*, 2008, 37(4), 326-332.
 62. Wang, J., Yau, W., Suwandy, A., Sung, E. Fusion of Palmprint and Palm Vein Images for Person Recognition Based on „Laplacianpalm“ Feature. *Proceedings of IEEE Computer Society Conference on Computer Vision and Pattern Recognition (IEEE CS CVPR)*, IEEE press, Minneapolis, MN, 2007, 1-8. <https://doi.org/10.1109/CVPR.2007.383386>
 63. Wang, J. G., Yau, W. Y., Suwandy, A., Sung, E. Person Recognition by Fusing Palmprint and Palm Vein Images Based on Laplacian Palm Representation. *Pattern Recognition*, 2008, 41(5), 1514-1527. <https://doi.org/10.1016/j.patcog.2007.10.021>
 64. Wang, L., Leedham, G., Cho, S.Y. Infrared Imaging of Hand Vein Patterns for Biometric Purposes. *IET Computer Vision*, 2007, 1(3-4), 113-122. <https://doi.org/10.1049/iet-cvi:20070009>
 65. Wang, R., Wang, G., Chen, Z., Zeng, Z., Wang, Y. A Palm Vein Identification System Based on Gabor Wavelet Features. *Neural Computing and Applications*, 2014, 24(1), 161-168. <https://doi.org/10.1007/s00521-013-1514-8>
 66. Wilson, C. *Vein Pattern Recognition: A Privacy-Enhancing Biometric*. Florida, US, CRC Press Publishers, 2010. <https://doi.org/10.1201/9781439821381>
 67. Wu, K., Lee, J., Lo, T., Chang, K., Chang, C. A Secure Palm Vein Recognition System. *The Journal of Systems and Software*, 2013, 86(11), 2870-2876. <https://doi.org/10.1016/j.jss.2013.06.065>
 68. Wu, W., Elliott, S. J., Lin, S., Yuan, W. Low-cost Biometric Recognition System Based on NIR Palm Vein Image. *IET Biometrics*, 2018, 8(3), 206-214. <https://doi.org/10.1049/iet-bmt.2018.5027>
 69. Wu, W., Yuan, W.Q., Lin, S. An Instrument of Palm Vein Pattern Recognition. *Applied Mechanics and Materials*, 2013, 333-335, 1092-1095. <https://doi.org/10.4028/www.scientific.net/AMM.333-335.1092>
 70. Wu, W., Yuan, W.Q., Song, H. A New Location Method of ROI for Contactless Palm Vein Recognition. *Advanced Materials Research*, 2013, 760-762, 1398-1401. <https://doi.org/10.4028/www.scientific.net/AMR.760-762.1398>
 71. Yakno, M., Saleh, J. M., Rosdi, B. A. Low Contrast Hand Vein Image Enhancement. *Proceedings of IEEE International Conference on Signal and Image Processing Applications (ICSIPA2011)*, IEEE press, Kuala Lumpur, Malaysia, 2011, 390-392. <https://doi.org/10.1109/ICSIPA.2011.6144135>
 72. Yan, X., Kang, W., Deng, F., Wu, Q. Palm Vein Recognition Based on Multi-Sampling and Feature-level Fusion. *Neurocomputing*, 2015, 151, 798-807. <https://doi.org/10.1016/j.neucom.2014.10.019>
 73. Yoruk, E., Dutagaci, H., Sankur, B. Hand Biometrics. *Image Vision and Computing*, 2006, 24(5), 483-497. <https://doi.org/10.1016/j.imavis.2006.01.020>
 74. Zhang, D., Guo, Z., Lu, G., Zhang, L., Liu, Y., Zuo, W. Online Joint Palmprint and Palmvein Verification. *Expert Systems with Applications*, 2011, 38(3), 2621-2631. <https://doi.org/10.1016/j.eswa.2010.08.052>
 75. Zhang, Y-B., Li, Q., You, J., Bhattacharya, P. Palm Vein Extraction and Matching for Personal Authentication. *Advances in Visual Information Systems*, Springer Berlin Heidelberg, 2007, 154-164. https://doi.org/10.1007/978-3-540-76414-4_16
 76. Zheng, Q., Tian, X., Yang, M., Wu, Y., Su, H. PAC-Bayesian Framework Based Drop-path Method for 2D Discriminative Convolutional Network Pruning. *Multi-dimensional Systems and Signal Processing*, 2020, 31. <https://doi.org/10.1007/s11045-019-00686-z>
 77. Zheng, Q., Yang, M., Tian, X., Jiang, N., Wang, D. A Full Stage Data Augmentation Method in Deep Convolutional Neural Network for Natural Image Classification. *Discrete Dynamics in Nature and Society*, 2020, 2020, 1-11. <https://doi.org/10.1155/2020/4706576>
 78. Zheng, Q., Yang, M., Yang, J., Zhang, Q., Zhang, X. Improvement of Generalization Ability of Deep CNN via Implicit Regularization in Two-Stage Training Process. *IEEE Access*, 2018, 6, 15844-15869. <https://doi.org/10.1109/ACCESS.2018.2810849>
 79. Zheng, Q., Zhao, P., Li, Y. Spectrum Interference-based Two-level Data Augmentation Method in Deep Learning for Automatic Modulation Classification. *Neural Computing and Applications*, 2021, 33, 7723-7745. <https://doi.org/10.1007/s00521-020-05514-1>

80. Zheng, Q., Zhao, P., Zhang, D., Wang, H. MR-DCAE: Manifold Regularization-based Deep Convolutional Auto-encoder for Unauthorized Broadcasting Identification. *International Journal of Intelligent Systems*, 2021, 36. <https://doi.org/10.1002/int.22586>
81. Zhixian, J., Qiang, L. Palm Vein Recognition Algorithm Using Curvelet and Wavelet. *Advanced Materials Research*, 2013, 710, 655-659. <https://doi.org/10.4028/www.scientific.net/AMR.710.655>
82. Zhong, D., Liu, S., Wang, W., Du, X. Palm Vein Recognition with Deep Hashing Network. *Pattern Recognition and Computer Vision*, Springer International Publishing, 2018, 38-49. https://doi.org/10.1007/978-3-030-03398-9_4
83. Zhou, C., Huang, J., Yang, F., Liu, Y. A Hybrid Fusion Model of Iris, Palm Vein and Finger Vein for Multi-biometric Recognition System. *Multimedia Tools and Applications*, 2020, 79, 29021-29042. <https://doi.org/10.1007/s11042-020-08914-6>
84. Zhou, Y., Kumar, A. Contactless Palm Vein Identification Using Multiple Representations. *Proceedings of IEEE Fourth International Conference on Biometrics: Theory, Applications and Systems*, Washington DC, 2010, 1-6. <https://doi.org/10.1109/BTAS.2010.5634470>
85. Zhou, Y., Kumar, A. Human Identification Using Palm-Vein Images. *IEEE Transactions on Information Forensics and Security*, 2011, 6(4), 1259-1274. <https://doi.org/10.1109/TIFS.2011.2158423>
86. Zuiderveld, K. J. *Graphic Gems IV-Contrast Limited Adaptive Histogram Equalization*. San Diego, CA, United States, Academic Press Professional, 1994, 474-485. <https://doi.org/10.1016/B978-0-12-336156-1.50061-6>



This article is an Open Access article distributed under the terms and conditions of the Creative Commons Attribution 4.0 (CC BY 4.0) License (<http://creativecommons.org/licenses/by/4.0/>).